HHS Public Access

Author manuscript

Oncogene. Author manuscript; available in PMC 2013 November 23.

Published in final edited form as:

Oncogene. 2013 May 23; 32(21): 2622–2630. doi:10.1038/onc.2012.284.

Arg/Abl2 promotes invasion and attenuates proliferation of breast cancer *in vivo*

Hava Gil-Henn, Ph.D.[*,1,#], **Antonia Patsialou, Ph.D.**[*,2], **Yarong Wang, M.Sc.**[2], **Michael Sloan Warren, M.Sc.**[1], **John S. Condeelis, Ph.D.**[2,3,&], and **Anthony J. Koleske, Ph.D.**[1,&]

[1]Department of Molecular Biophysics & Biochemistry, Yale University, 333 Cedar Street, New Haven, CT 06520, USA

[2]Department of Anatomy and Structural Biology, Albert Einstein College of Medicine, 1301 Morris Park Avenue, Bronx, NY 10461, USA

[3]Gruss Lipper Biophotonics Center, Albert Einstein College of Medicine, 1301 Morris Park Avenue, Bronx, NY 10461, USA

Abstract

Tumor progression is a complex, multistep process involving accumulation of genetic aberrations and alterations in gene-expression patterns leading to uncontrolled cell division, invasion into surrounding tissue and finally dissemination and metastasis. We have previously shown that the Arg/Abl2 non-receptor tyrosine kinase acts downstream of the EGF receptor and Src tyrosine kinases to promote invadopodium function in breast cancer cells, thereby promoting their invasiveness. However, whether and how Arg contributes to tumor development and dissemination *in vivo* has never been investigated. Using a mouse xenograft model, we show that knocking down Arg in breast cancer cells leads to increased tumor cell proliferation and significantly enlarged tumor size. Despite having larger tumors, the Arg knockdown tumor-bearing mice exhibit significant reductions in tumor cell invasion, intravasation into blood vessels, and spontaneous metastasis to lungs. Interestingly, we found that proliferation-associated genes in the Ras-MAPK pathway are upregulated in Arg-knockdown breast cancer cells, as is Ras-MAPK signaling, while invasion-associated genes are significantly downregulated. These data suggest that Arg promotes tumor cell invasion and dissemination, while simultaneously inhibiting tumor growth. We propose that Arg acts as a switch in metastatic cancer cells that governs the decision to “grow or go” (divide or invade).

Keywords

breast cancer; metastasis; invasion; proliferation; Arg kinase

[&]*Correspondence should be addressed to:* John Condeelis: Tel: (718) 678-1126, Fax: (718) 678-1128, john.condeelis@einstein.yu.edu Anthony Koleske: Tel: (203) 785-5624, Fax (203) 785-7979, anthony.koleske@yale.edu.

[#]Current address: Bar-Ilan University School of Medicine, 8 Henriyetta Sold Street, Safed 13115, Israel

[*]Equal contribution, co-first authors

CONFLICT OF INTEREST The authors declare no conflict of interest.

INTRODUCTION

Malignant transformation is a complex, multistep process resulting from accumulated genetic alterations that drive changes in cellular signaling and behavior. During this process, tumor cells acquire the capacity for sustained proliferative signaling, replicative immortality, resistance to apoptosis, and for inducing local angiogenesis (1, 2). Tumors progress to a metastatic stage by responding to microenvironmental signals that promote invasion and migration, and consequently escaping the primary tumor (3). Tumor cells that have succeeded in these previous stages proceed by penetrating the basement membrane, intravasating through the vascular subendothelial basement membrane into blood vessels, surviving the physical stress generated by blood flow, evading destruction by the immune system, and finally by extravasating into a target organ. Upon reaching a new microenvironment, tumor cells accumulate additional adaptive changes that allow them to grow and to form a new metastatic colony (1, 2, 4). Primary tumors can often be surgically removed and are usually responsible for only a small percentage of cancer deaths. Complications associated with distant metastasis are the primary cause of mortality from cancer and therefore serves as an important target for potential therapeutic intervention.

The mammalian Abelson family of non-receptor tyrosine kinases, which includes c-Abl (Abl) and Abl-related gene (Arg), are essential transducers of signals from cell surface growth factor and adhesion receptors to the cell proliferation and cytoskeletal control machineries (5, 6). Abl and Arg regulate several biological processes including cell motility and morphogenesis, response to genotoxic stress, and apoptosis (5). Emerging evidence indicate that signaling by Abl family kinases also regulate development and function of the immune and nervous systems (7) and mediate cytoskeletal rearrangements required for microbial pathogenesis (8, 9).

Abl family kinases were first identified as oncogenes associated with human leukemias. Oncogenic activation of Abl is most commonly associated with a chromosomal translocation that fuses sequences encoding a portion of the Bcr protein to the N-terminal part of Abl, resulting in a hybrid gene encoding the Bcr-Abl oncoprotein. Similarly, Arg is activated by fusion with the Tel transcription factor in rare cases of AML (10-13). These translocations mediate oligomerization of Abl and Arg, respectively, leading to increased tyrosine kinase activity. Hematopoietic cells expressing these activated oncoproteins exhibit decreased adhesiveness and premature release from the bone marrow stroma accompanied by increased ability to survive, proliferate, migrate and invade (14).

Recent reports suggest that activation of Abl kinases may also play a role in solid tumor development. Increased levels of Abl and Arg or elevated Abl and Arg activities have been detected in non-small cell lung cancers (15), anaplastic thyroid cancers (16), melanoma (17) and in advanced colorectal and pancreatic cancers (18, 19). Increased expression and activity of the Abl kinase family was also reported in highly invasive breast cancer cell lines, where they regulate proliferation, survival, and invasion downstream of deregulated EGFR, Her2, IGFR, and Src kinases (20-23). However, many of these studies have focused primarily on the role for Abl or overlapping roles for Abl and Arg in these cancers. We have recently shown that Arg, but not Abl, localizes to invadopodia, F-actin-rich protrusions that

mediate matrix degradation, in invasive breast cancer cells. Within invadopodia, Arg acts downstream of the EGF receptor and Src kinases to phosphorylate cortactin, which triggers actin polymerization, stimulates invadopodial function, and promotes matrix degradation and invasive cell migration (24). In addition, when assaying a panel of breast cancer cell lines, Arg was found to be preferentially overexpressed and activated in the most invasive estrogen receptor (ER)-negative cell lines compared to the less aggressive luminal ER-positive cell lines (21). These data strongly suggest that Arg may have a specific role in invasion and metastasis of breast cancer *in vivo*.

Here, we employ a mouse xenograft model to determine how the loss of Arg function affects human breast cancer tumorigenesis, invasion and metastasis. We find that Arg knockdown (Arg KD) MDA-MB-231 cells proliferate more extensively, leading to significantly larger tumors than control MDA-MB-231 cells. Despite the greatly increased tumor size, significantly fewer cells escape from Arg KD tumors *in vivo*. In addition, mice bearing orthotopic tumors derived from Arg KD cells have fewer tumor cells in their blood circulation and significantly fewer lung metastases. Interestingly, we found that proliferation-associated genes in the Ras-MAPK pathway and Ras-MAPK signaling were upregulated in Arg KD cells, while genes associated with the invasive migration machinery were significantly downregulated. These data suggest that Arg kinase helps determine the balance between proliferation and invasion in breast cancer cells *in vivo*.

RESULTS

Arg knockdown in breast tumor cells increases primary tumor size due to enhanced cell proliferation

For our study, we used the MDA-MB-231 cell line, an ATCC-established human breast adenocarcinoma cell line that is widely used for studying metastasis because of its ability to grow orthotopic tumors that spontaneously metastasize to the lungs in mice. In addition, its triple-negative status (estrogen/progesterone receptor negative, HER2 negative) categorizes it in the basal-like subtype of breast cancers, the most aggressive, highly metastatic breast tumors in patients (25). We generated stable knockdown of the ARG/ABL2 gene in the MDA-MB-231 cells using two distinct shRNA sequences (Arg KD1 and Arg KD2 cell lines) or an empty vector as control (pSR cell line). As shown in Figure 1A, both knockdown sequences resulted in a >95% knockdown of Arg expression, without affecting expression of the closely related Abl and Src kinases.

To test how the loss of Arg affects cancer progression *in vivo*, we injected the stable Arg KD1 and Arg KD2 cell lines into the mammary gland of severe combined immunodeficiency (SCID) mice. Tumors arising from the Arg KD cell lines were significantly bigger than tumors from the control cell line (Figure 1B and 1C). To gain insights into the mechanism for this more rapid tumor growth, we used histological markers to investigate the cellular composition of the tumors. No differences in general inflammation, necrosis, or blood vessel composition were noted in the Arg KD1 tumors (Figure 2A-C). We noted a 2-fold increase in the percentage of proliferating Ki67-positive cells in Arg KD1 tumors compared with control tumors (Figure 2D-E), while apoptosis sensitivity *in vivo* was not overall decreased (Figure S1). Consistent with this finding, both

Arg KD1 and Arg KD2 cell lines exhibit a modest but significantly elevated proliferation rate in culture compared with control cells (Figure 2F). Together, these results suggest that loss of Arg in breast tumor cells promotes proliferation *in vitro* and *in vivo*.

Arg knockdown decreases tumor cell invasion both in vitro and in vivo

We and others have previously shown that Arg promotes *in vitro* breast cancer cell invasion by regulating the maturation of invadopodia, F-actin rich protrusions that are believed to mediate penetration of escaping tumor cells through basement membrane and extracellular matrix (23, 24). We first verified the decreased potential of the stable Arg KD1 and Arg KD2 cell lines to invade through a Matrigel-coated Boyden chamber. Indeed, both Arg knockdown cell lines showed significantly reduced invasion *in vitro* compared to the control cell line (Figure 3A). This effect was specific to invasion through matrix, since migration through uncoated chambers was not affected in the Arg KD1 and Arg KD2 cell lines (Figure 3B).

We next sought to determine whether Arg controls invasion *in vivo*, in the context of the primary tumor. For this purpose, we used the *in vivo* invasion assay (26), with which we have previously shown that invasive tumor cells can be collected from parental MDA-MB-231 primary tumors in response to EGF (27). We used this method here to measure invasion in control and Arg KD1-derived primary tumors. In agreement with our *in vitro* data, the total number of tumor cells invading towards EGF in the Arg KD1 tumors was significantly reduced compared to control tumors of the same volume (Figure 3C).

We also injected the Abl/Arg inhibitor STI-571 into mice bearing tumors composed of MDA-MB-231 parental cells prior to needle insertion. This method allows us to test how application of an Abl family kinase inhibitor affects invasion of parental MDA-MB-231 cells, thereby excluding potential complications from the altered growth of the Arg knockdown tumor cells. Indeed, application of STI-571 to parental MDA-MB-231 orthotopic tumors significantly reduced invasion by tumor cells *in vivo*, in agreement with the reduced invasion in the Arg KD1 primary tumors (Figure 3D). Together, these observations indicate that reduced Arg function significantly compromises tumor cell invasion both *in vitro* and *in vivo*.

Arg knockdown significantly abrogates tumor cell dissemination

Given the reduced invasive properties of Arg KD1 tumor cells, we next tested how subsequent steps in metastasis were affected. Using an established intravasation assay (28), we found that both Arg KD1 and Arg KD2 tumor-bearing mice had significantly fewer circulating tumor cells in their blood, as compared to mice bearing control tumors of similar size (Figure 3E). Similarly, STI-571-treated mice bearing parental MDA-MB-231 tumors also showed fewer circulating tumor cells in their blood compared to mice treated with only DMSO vehicle control (Figure 3F). This later finding suggests that Arg kinase activity is necessary for intravasation of tumor cells into the bloodstream.

Arg knockdown compromises spontaneous lung metastasis but does not affect extravasation

To establish metastases, tumor cells must extravasate into the target organ and establish a new metastatic colony. When testing for the effect of Arg in pulmonary metastasis, mice bearing Arg KD1 or Arg KD2 orthotopic tumors exhibited significantly fewer lung metastases than control mice bearing equal size tumors (Figure 4A-C). This is in agreement with the reduced number of both invasive primary tumor cells (Figure 3C) and circulating tumor cells (Figure 3E) in these mice. An alternative explanation for the reduction in spontaneous lung metastasis could potentially be a reduction in survival of the Arg KD cells in the blood circulation due to mechanical stress. We therefore also measured the ability of control and Arg KD1 cells to establish lung metastases when injected directly into the tail vein (Figure 4D). In this assay, tumor cells are artificially introduced directly into the bloodstream bypassing the requirement for invasion and intravasation in the primary tumor. Subsequent quantification of metastases measures only the ability of cells to survive in blood circulation and to extravasate and colonize the lung. First, we measured single extravasated tumor cells in the lungs at 48 hours post-injection, when it has been shown that MDA-MB-231 cells are extravascular but not yet replicated (29). Both control and Arg KD1 cells showed similar number of extravasated tumor cells in the lungs (Fig. 4D-F), suggesting that the ArgKD1 cells show no difference in either survival capacity in the blood or capacity to extravasate in the lungs compared to the control cells. We also measured metastatic colonies in the lungs at 4 weeks post-injection of the tumor cells in the tail vein. Under these conditions, Arg KD1 cells showed a significant increase in lung metastases compared to control cells (Figure 4G), most likely due to their proliferative advantage. These data strongly suggest that whereas Arg plays a crucial role in breast cancer metastasis by promoting invasion and intravasation in the primary tumor, it is not necessary for extravasation or establishment of tumors in the target organ of metastasis.

Loss of Arg function differentially affects invasion and proliferation pathways in breast cancer cells

Previous microarray analyses suggest that genes involved in cell growth and proliferation are highly upregulated in primary breast tumors (reviewed in: (30)). However, targeted analyses have demonstrated that tumor cells that escape the primary tumor downregulate proliferation genes, but upregulate genes related to EGF-induced motility pathways (3, 31, 32). We report above that loss of Arg in breast cancer cells results in increased proliferation, while significantly decreasing invasion, suggesting that Arg might have different effects on these two processes.

To further validate this hypothesis, we measured the relative mRNA levels of genes involved in EGFR-mediated proliferation or invasion pathways by quantitative PCR. As shown in Figure 5A and Table S1, expression of genes associated with proliferation pathways was significantly increased in both the Arg KD1 and Arg KD2 cell lines relative to control cells, while expression of motility-related genes was significantly decreased.

Because they exhibit increased transcription of Ras-MAPK-related genes (Figure 5A), greater proliferation, and produce larger primary tumors (Figures 1B-C and 2F), we further

analyzed the status of the Ras-MAPK signaling pathway in ArgKD1 and ArgKD2 cells. Both Ras protein levels and Ras activity were increased in the Arg KD1 and Arg KD2 cell lines compared to the control cells (Figures 5B-C). In addition, MAPK phosphorylation was significantly increased in both Arg knockdown cell lines compared to control cells (Figures 5D-E), further indicating regulation of MAPK-mediated proliferation pathways by Arg. MAPK activity was also increased in tumor sections derived from ArgKD1 tumors relative to control tumors (Figures 5F-G). In addition to the reduced expression of invasive migration signaling components observed, we have recently shown that the loss of Arg function compromises tumor cell invasion by preventing EGFR-mediated cortactin phosphorylation and invadopodia function in breast cancer cell invadopodia (24). Collectively, these observations suggest that Arg acts to attenuate proliferation while stimulating invasion in breast tumor cells.

DISCUSSION

Tumor growth and metastasis are complementary processes requiring a combination of spontaneous genetic changes that increase proliferation in the primary cancer cells, and that create microenvironments that initiate increased motility and invasion. Here, we provide evidence that the Arg/Abl2 non-receptor tyrosine kinase attenuates proliferation, while promoting invasion and metastasis. Knockdown of Arg in breast tumor cells promotes cell proliferation, leading to larger tumor size, while significantly decreasing subsequent progression stages of metastasis, namely invasion, intravasation, and lung metastasis. Arg may therefore regulate a stage in which tumor cells, as a response to micro-environmental signals, may stop proliferating and start invading.

Tumor size is currently one criterion used in the American Joint Committee on Cancer (AJCC) staging system for determining treatment options for patients (33). Indeed, several research studies in mouse models have linked the increased ability of tumor cells to metastasize with larger tumor size. These studies suggested that increased expression of specific metastatic genes gives the primary tumor advantage in growth, which enables further selection and expansion of a metastatic pool of cells containing the same gene (34, 35). However in the present study, we found that Arg-deficient tumor cells produce significantly larger tumors that do not metastasize, suggesting that the processes of invasion and proliferation may be coordinated through signaling by Arg. To our knowledge, this is the first demonstration that tumor growth and invasion can be oppositely regulated in a mouse mammary xenograft model. Consistent with these findings, one of our groups has previously shown that actively migrating invasive tumor cells downregulate proliferation-associated gene expression while upregulating genes that encode for motility and invasion (3, 31, 32).

The opposite correlation of invasion and proliferation in our study may seem to be contradictory to the predictive role of tumor size in patient survival outcome or to the studies that show that “metastasis signatures” are associated with tumor size. This contradiction could be partly explained by the different experimental techniques used in the latter studies, where metastasis was measured after tail vein injection of breast tumor cells and/or by whole-body bioluminescence imaging in mice (34, 35). Both these assays in essence

measure growth in the metastatic milieu rather than invasion and dissemination of tumor cells; experimental metastasis measures extravasation and growth of the tumor cells in the lungs, while bioluminescence imaging is not sensitive enough to image single-disseminated cells and therefore only grown colonies are imaged. Similarly in patients, only metastases that have grown into tumors can be detected by medical imaging and not singly disseminated cells, and therefore it is not surprising that cell proliferation pathways are linked to clinical recurrence.

In our experimental model, we dissected the different steps in metastasis using specific assays to measure tumor growth, *in vivo* invasion, intravasation, extravasation, and lung colonization, yielding more detailed information on specific steps of metastasis. Our studies revealed critical roles for Arg as an attenuator of cell proliferation and a promoter for spontaneous invasion, intravasation, and metastasis. Similar to our finding that Arg knockdown increases tumor growth, Allington *et al*. have recently reported that mouse mammary tumors treated with STI-571 are larger compared to tumors treated with vehicle only (36). Interestingly, experimental metastasis following tail vein injection of Arg KD cells was increased. Considering that Arg KD cells have increased growth capabilities, it is not surprising that they established more metastatic colonies in the lungs when artificially introduced straight into the bloodstream. Overall, our data suggests that proliferation and invasion may be coordinately regulated by Arg in breast cancer cells *in vivo*. Interestingly, and in line with our findings, a recent clinical analysis of breast cancer patients demonstrated that in extensive node-positive disease, very small tumor size rather than larger tumors may predict higher breast cancer specific mortality (37).

Cell growth is regulated by restriction points in the cell cycle. When cells complete mitosis and enter the G1 phase, the decision to progress to S phase or to arrest growth must be made. We hypothesize that proliferating cells do not invade as the process of cell movement may not be compatible with the process of cytokinesis. It is possible that Arg directly antagonizes progression through G1, as has been shown for Abl following its overexpression in fibroblasts (38). Whether and how Arg activity is mechanistically coupled to cell cycle progression is currently unknown and a subject for future studies.

We propose here that invasion and proliferation are opposing functions of tumor cells. Most likely, cues from the tumor microenvironment of the primary tumor dictate whether a cell will grow or migrate at a certain time and space. Our data suggest that Arg may have a role in determining this switch between proliferation and invasion.

MATERIALS AND METHODS

Antibodies

The following antibodies were used for immunoblotting: Anti-Abl (Santa Cruz), anti-Src (Calbiochem), anti-actin (Millipore), anti-MAP kinase (Cell Signaling) and anti-phospho MAP kinase (Cell Signaling), anti-Ras (Cell Signaling). Anti-Arg antibody was a generous gift from Dr. Peter Davis (Albert Einstein School of Medicine, New York City, NY). For histology, anti-Ki67 (Vector) and anti-endomucin (Santa Cruz) antibodies were also used.

Cell lines

MDA-MB-231 cells (ATCC) were cultured in DMEM supplemented with 10% fetal bovine serum (FBS) and antibiotics (Invitrogen). shRNA cell lines (Arg KD1 and Arg KD2) were generated by cloning two different specific knockdown sequences for Arg into the pSuper-retro retroviral plasmid (ArgKD1: 5′- GTC CTT ATC TCA CCC ACT C -3′ and ArgKD2: 5′- CCT CAA ACT CGC AAC AAA T -3′). The retroviral plasmid was transfected into the Phoenix Amphotrophic packaging cell line, and retroviral sups were used to infect MDA-MB-231, that were then selected with 10 μg/ml puromycin. A control cell line (pSR) was also generated by transfection of empty vector using the same protocol. The magnitude of Arg knockdown was determined by quantitative immunoblotting.

Western Blot

Cells were washed in cold PBS and lysed in modified RIPA buffer (50mM Tris pH 7.2, 150 mM NaCl, 1% NP-40, 0.5% deoxycholate, 0.1% SDS, 1 mM EDTA, 2mM NaF, 1mM Na_3VO_4, and protease inhibitors). Samples were resolved by SDS-PAGE, transferred to nitrocellulose, blocked in odyssey blocking solution (LiCor), incubated in primary antibodies overnight at 4°C, secondary antibodies for 1 hour at RT, and finally analyzed using the Odyssey (LiCor). Visualization and processing of images was performed with ImageJ (NIH). Blots were quantified using the Quantity One software (BioRad).

Ras activity assay

Endogenous Ras-GTP levels were measured using an enzyme-linked immunosorbent assay (ELISA)-based G-LISA kit (Cytoskeleton, Inc #BK131) following the manufacturer's instructions. Briefly, cells were plated and allowed to grow to roughly 70% confluence before being washed with PBS and lysed in 700 μl of ice-cold lysis buffer in the presence of protease and phosphatase inhibitors. The lysate was clarified by centrifugation at 10,000 × g for 1 min, and snap-frozen in liquid nitrogen. After normalizing protein concentration using PrecisionRed (Cytoskeleton, Inc), samples were added in triplicate to wells coated with a Ras GTP-binding protein and incubated at 4° for 30 minutes at 400 RPM. After washing, bound Ras GTP levels were determined by subsequent incubations with an anti-Ras antibody and a secondary HRP-conjugated antibody, followed by addition to an HRP detection reagent. Background was determined by a negative control well, and signal was normalized to an internal control of .5 ng of activated Ras. Experiments for each cell type were repeated three times.

In vitro proliferation

5×10^4 cells were plated in duplicates in 6 well plates containing DMEM/10% FBS and counted in duplicates every other day for 8 days. Experiments were repeated at least three times.

Transwell invasion assay

Invasion was evaluated by plating 2.5×10^4 cells in the upper chambers of 8.0 μm pore size reduced growth factor Matrigel chambers or control non-coated chambers (BD Biosciences) in 0.5% FBS/DMEM. Cells were allowed to invade for 24 hours towards DMEM/10% FBS,

fixed with ice-cold methanol, and stained with 0.5% crystal violet. Two chambers per condition in 3 independent experiments were imaged at 5x and four fields per chamber were counted and analyzed. The invasion index was calculated as number of cells invaded via proteolysis normalized to number of cells that migrated in uncoated plates.

Mouse Xenograft Model

All procedures were conducted in accordance with the National Institutes of Health regulations, and approved by the Albert Einstein College of Medicine and the Yale animal care and use committees. A total of 2×10^6 MDA-MB-231 cells (either parental, pSR vector control, or Arg shRNA knockdown cells) per animal were resuspended in sterile PBS with 20% collagen I (BD Biosciences) and injected into the lower left mammary gland of SCID mice (NCI, Frederick, MD). All experiments, unless otherwise stated, were performed on tumors that were 1-1.2 cm in diameter.

For inhibitor treatments, mice were injected intraperitoneally four hours prior to experiments with 200 mg/kg of STI-571 (LC Laboratories), or equal volume of DMSO vehicle control. For histology and immunostaining experiments, primary tumors were excised at 1-1.2 cm diameter, fixed in formalin, and paraffin embedded. Sections from the middle of the primary tumors were stained with hematoxylin and eosin (H&E) for general histology, or immunostained with specific antibodies (anti-Ki67 for proliferation or anti-endomucin for blood vessels). Briefly, samples for immunohistochemistry (IHC) were sectioned at 5μm, deparaffinized in xylene followed by graded alcohols. Antigen retrieval was performed in 10mM sodium citrate buffer at pH 6.0, heated to 96C, for 20 min. Endogenous peroxidase activity was quenched using 3% hydrogen peroxide in PBS for 10 min. Blocking was performed by incubating sections in 5% normal donkey serum with 2%BSA for 1 hr. Primary antibodies were: rabbit polyclonal anti-Ki67 (VP-K451, Vector), rat monoclonal anti-endomucin (sc-65495, Santa Cruz Biotechnology), rabbit polyclonal anti-p44/42 MAPK (9102, Cell Signaling) and rabbit monoclonal anti-phospho-p44/42 MAPK (4370, Cell Signaling). Tumor sections were stained by routine IHC methods, using HRP rabbit polymer conjugate (Invitrogen), for 20 minutes to localize the antibody bound to antigen, with diaminobenzidine as the final chromogen. All immunostained sections were lightly counterstained with hematoxylin. Proliferation was quantified by counting the Ki67-positive cells (brown) over total number of cells (blue) in five representative fields per tumor (at 40x), and total three tumors per group. Blood vessels were quantified by counting positive cells per field in five representative fields per tumor (at 10x) and total three tumors per group. Necrotic tumor areas were excluded from the analysis (no significant difference in overall necrosis was seen between cell lines).

In vivo invasion assay

Cell collection into needles placed into live anesthetized animals was performed as previously described (26). Briefly, 33-gauge needles were filled with Matrigel and L15-BSA with or without addition of 25 nM human recombinant EGF (Invitrogen). Mice were anesthesized using 5% isoflurane and laid on their back. The isofluorane was reduced to 2%, and a small patch of skin over the tumor was removed. Six 25-gauge guide needles with blocking wires were inserted to a depth of 2 mm from both sides of the tumor. Blocking

wires were then removed, and one Matrigel-filled 33 gauge needle (either with or without EGF) was inserted into each guide needle. The needles were left in the tumor for 4 hours. Isofluorane concentration was slowly lowered to 0.5% during the course of experiment to keep the mouse breathing even and unlabored. After 4 hours of collection, the needles are removed and the total number of cells collected was determined by 4′,6-diamidino-2-phenylindole (DAPI) staining.

Intravasation assay

The number of circulating tumor cells was measured in mice bearing a tumor of 1-1.2 cm as previously described (28). Briefly, blood was drawn from the right heart ventricle of anesthetized mice and whole blood was plated in DMEM/20% FBS. Tumor cells were counted after one week. As a control, blood from non-tumor bearing mice was plated as well and the complete absence of epithelial tumor cells was confirmed.

Lung metastasis assays

Spontaneous lung metastases were measured in SCID mice bearing orthotopic pSR control, ArgKD1 and ArgKD2 MDA-MB-231 derived tumors of equal size (1-1.2 cm in diameter). The lungs were excised, fixed in formalin, paraffin embedded and then serially sectioned (50 μm interval) and stained for hematoxylin and eosin (H&E). Total metastatic colonies from the first eight sections of each lung sample were quantified.

The ability of tumor cells to metastasize after direct injection into the blood was determined after injection of 400,000 pSR control or Arg KD1 cells in the tail vein of SCID mice. Four weeks following injection, mice were sacrificed and their lungs were excised, fixed, embedded, sectioned and stained with H&E as above. For quantification, the total number of metastatic colonies from the middle section of each lung sample was quantified. To directly test the cells' relative abilities to extravasate (without respect to growth potential), a separate experiment was performed where single extravasated tumor cells were counted in the lungs. 400,000 pSR or ArgKD1 cells were labeled with green cell tracker dye (Invitrogen) and injected in the tail vein of SCID mice. Extravasation was evaluated at 48 hours post-injection, when MDA-MB-231 cells have been shown to be extravasated but not yet replicated (29). To validate that the cells were indeed extravascular, blood vessels were visualized in the mice by tail vein injection of rhodamine-conjugated lectin (Vector Laboratories) 5 minutes before sacrifice. The largest lung lobe of each mouse was imaged using an Olympus FV1000-MPE multiphoton microscope and single extravascular cells were counted.

RNA extraction and PCR amplification

RNA was extracted from triplicate plates of pSR and ArgKD cells with the RNeasy Mini kit (Qiagen). The quality of total RNA was evaluated by electrophoresis on 1% agarose gels and ethidium bromide staining. 1 μg of total RNA was reverse transcribed using SuperScript II (Invitrogen) and oligo(dT) primers. Quantitative PCR analysis was performed as previously described (31), using the Power SYBR Green PCR Core Reagents system (Applied Biosystems) and gene sequence-specific primers (Table S2). Each PCR reaction was performed in triplicate, and the mean threshold cycle (CT) values were used for

analysis. GAPDH was used as a housekeeping gene control. Results were evaluated with the ABI Prism SDS 2.1 software.

Supplementary Material

Refer to Web version on PubMed Central for supplementary material.

ACKNOWLEDGEMENTS

We would like to thank the Einstein Histotechnology and Comparative Pathology Facility for their excellent service and to Dr. Rani Sellers for helpful advice and suggestions. This work was supported by PHS grant CA133346 and an Exceptional Project Award from the Breast Cancer Alliance (A.J.K.) and CA100324 (J.S.C.).

REFERENCES

1. Hanahan D, Weinberg RA. The hallmarks of cancer. Cell. 2000; 100(1):57–70. Epub 2000/01/27. [PubMed: 10647931]
2. Hanahan D, Weinberg RA. Hallmarks of cancer: the next generation. Cell. 2011; 144(5):646–74. Epub 2011/03/08. [PubMed: 21376230]
3. Wang W, Goswami S, Sahai E, Wyckoff JB, Segall JE, Condeelis JS. Tumor cells caught in the act of invading: their strategy for enhanced cell motility. Trends Cell Biol. 2005; 15(3):138–45. [PubMed: 15752977]
4. Nguyen DX, Bos PD, Massague J. Metastasis: from dissemination to organ-specific colonization. Nat Rev Cancer. 2009; 9(4):274–84. Epub 2009/03/25. [PubMed: 19308067]
5. Bradley WD, Koleske AJ. Regulation of cell migration and morphogenesis by Abl-family kinases: emerging mechanisms and physiological contexts. J Cell Sci. 2009; 122(Pt 19):3441–54. Epub 2009/09/18. [PubMed: 19759284]
6. Pendergast AM. The Abl family kinases: mechanisms of regulation and signaling. Adv Cancer Res. 2002; 85:51–100. Epub 2002/10/11. [PubMed: 12374288]
7. Derkinderen P, Scales TM, Hanger DP, Leung KY, Byers HL, Ward MA, et al. Tyrosine 394 is phosphorylated in Alzheimer's paired helical filament tau and in fetal tau with c-Abl as the candidate tyrosine kinase. J Neurosci. 2005; 25(28):6584–93. Epub 2005/07/15. [PubMed: 16014719]
8. Backert S, Feller SM, Wessler S. Emerging roles of Abl family tyrosine kinases in microbial pathogenesis. Trends Biochem Sci. 2008; 33(2):80–90. Epub 2008/01/10. [PubMed: 18182299]
9. Newsome TP, Weisswange I, Frischknecht F, Way M. Abl collaborates with Src family kinases to stimulate actin-based motility of vaccinia virus. Cell Microbiol. 2006; 8(2):233–41. Epub 2006/01/31. [PubMed: 16441434]
10. Advani AS, Pendergast AM. Bcr-Abl variants: biological and clinical aspects. Leuk Res. 2002; 26(8):713–20. Epub 2002/08/23. [PubMed: 12191565]
11. Cazzaniga G, Tosi S, Aloisi A, Giudici G, Daniotti M, Pioltelli P, et al. The tyrosine kinase abl-related gene ARG is fused to ETV6 in an AML-M4Eo patient with a t(1;12)(q25;p13): molecular cloning of both reciprocal transcripts. Blood. 1999; 94(12):4370–3. Epub 1999/12/10. [PubMed: 10590083]
12. Iijima Y, Ito T, Oikawa T, Eguchi M, Eguchi-Ishimae M, Kamada N, et al. A new ETV6/TEL partner gene, ARG (ABL-related gene or ABL2), identified in an AML-M3 cell line with a t(1;12)(q25;p13) translocation. Blood. 2000; 95(6):2126–31. Epub 2000/03/09. [PubMed: 10706884]
13. McWhirter JR, Wang JY. Activation of tyrosinase kinase and microfilament-binding functions of c-abl by bcr sequences in bcr/abl fusion proteins. Mol Cell Biol. 1991; 11(3):1553–65. Epub 1991/03/01. [PubMed: 1705008]
14. Chopra R, Pu QQ, Elefanty AG. Biology of BCR-ABL. Blood Rev. 1999; 13(4):211–29. Epub 2000/03/31. [PubMed: 10741897]

15. Rikova K, Guo A, Zeng Q, Possemato A, Yu J, Haack H, et al. Global survey of phosphotyrosine signaling identifies oncogenic kinases in lung cancer. Cell. 2007; 131(6):1190–203. Epub 2007/12/18. [PubMed: 18083107]
16. Podtcheko A, Ohtsuru A, Tsuda S, Namba H, Saenko V, Nakashima M, et al. The selective tyrosine kinase inhibitor, STI571, inhibits growth of anaplastic thyroid cancer cells. J Clin Endocrinol Metab. 2003; 88(4):1889–96. Epub 2003/04/08. [PubMed: 12679488]
17. Ganguly SS, Fiore LS, Sims JT, Friend JW, Srinivasan D, Thacker MA, et al. c-Abl and Arg are activated in human primary melanomas, promote melanoma cell invasion via distinct pathways, and drive metastatic progression. Oncogene. 2012; 31(14):1804–16. Epub 2011/09/06. [PubMed: 21892207]
18. Chen WS, Kung HJ, Yang WK, Lin W. Comparative tyrosine-kinase profiles in colorectal cancers: enhanced arg expression in carcinoma as compared with adenoma and normal mucosa. Int J Cancer. 1999; 83(5):579–84. Epub 1999/10/16. [PubMed: 10521789]
19. Crnogorac-Jurcevic T, Efthimiou E, Nielsen T, Loader J, Terris B, Stamp G, et al. Expression profiling of microdissected pancreatic adenocarcinomas. Oncogene. 2002; 21(29):4587–94. Epub 2002/06/27. [PubMed: 12085237]
20. Sirvent A, Benistant C, Roche S. Cytoplasmic signalling by the c-Abl tyrosine kinase in normal and cancer cells. Biol Cell. 2008; 100(11):617–31. Epub 2008/10/15. [PubMed: 18851712]
21. Srinivasan D, Plattner R. Activation of Abl tyrosine kinases promotes invasion of aggressive breast cancer cells. Cancer Res. 2006; 66(11):5648–55. Epub 2006/06/03. [PubMed: 16740702]
22. Srinivasan D, Sims JT, Plattner R. Aggressive breast cancer cells are dependent on activated Abl kinases for proliferation, anchorage-independent growth and survival. Oncogene. 2008; 27(8): 1095–105. Epub 2007/08/19. [PubMed: 17700528]
23. Smith-Pearson PS, Greuber EK, Yogalingam G, Pendergast AM. Abl kinases are required for invadopodia formation and chemokine-induced invasion. J Biol Chem. 2010; 285(51):40201–11. Epub 2010/10/13. [PubMed: 20937825]
24. Mader CC, Oser M, Magalhaes MA, Bravo-Cordero JJ, Condeelis J, Koleske AJ, et al. An EGFR-Src-Arg-Cortactin Pathway Mediates Functional Maturation of Invadopodia and Breast Cancer Cell Invasion. Cancer Res. 2011; 71(5):1730–41. Epub 2011/01/25. [PubMed: 21257711]
25. Brenton JD, Carey LA, Ahmed AA, Caldas C. Molecular classification and molecular forecasting of breast cancer: ready for clinical application? J Clin Oncol. 2005; 23(29):7350–60. Epub 2005/09/08. [PubMed: 16145060]
26. Wyckoff JB, Segall JE, Condeelis JS. The collection of the motile population of cells from a living tumor. Cancer research. 2000; 60(19):5401–4. Epub 2000/10/18. [PubMed: 11034079]
27. Patsialou A, Wyckoff J, Wang Y, Goswami S, Stanley ER, Condeelis JS. Invasion of human breast cancer cells in vivo requires both paracrine and autocrine loops involving the colony-stimulating factor-1 receptor. Cancer Res. 2009; 69(24):9498–506. Epub 2009/11/26. [PubMed: 19934330]
28. Wyckoff JB, Jones JG, Condeelis JS, Segall JE. A critical step in metastasis: in vivo analysis of intravasation at the primary tumor. Cancer Res. 2000; 60(9):2504–11. [PubMed: 10811132]
29. Gupta GP, Nguyen DX, Chiang AC, Bos PD, Kim JY, Nadal C, et al. Mediators of vascular remodelling co-opted for sequential steps in lung metastasis. Nature. 2007; 446(7137):765–70. Epub 2007/04/13. [PubMed: 17429393]
30. Whitfield ML, George LK, Grant GD, Perou CM. Common markers of proliferation. Nat Rev Cancer. 2006; 6(2):99–106. Epub 2006/02/24. [PubMed: 16491069]
31. Wang W, Goswami S, Lapidus K, Wells AL, Wyckoff JB, Sahai E, et al. Identification and testing of a gene expression signature of invasive carcinoma cells within primary mammary tumors. Cancer Res. 2004; 64(23):8585–94. [PubMed: 15574765]
32. Wang W, Wyckoff JB, Goswami S, Wang Y, Sidani M, Segall JE, et al. Coordinated regulation of pathways for enhanced cell motility and chemotaxis is conserved in rat and mouse mammary tumors. Cancer Res. 2007; 67(8):3505–11. Epub 2007/04/19. [PubMed: 17440055]
33. Greene, FL.; Balch, CM.; Haller, DG.; Morrow, M. AJCC Cancer Staging Manual. 6th edition. Springer; Chicago, IL: 2002.
34. Minn AJ, Gupta GP, Siegel PM, Bos PD, Shu W, Giri DD, et al. Genes that mediate breast cancer metastasis to lung. Nature. 2005; 436(7050):518–24. Epub 2005/07/29. [PubMed: 16049480]

35. Minn AJ, Gupta GP, Padua D, Bos P, Nguyen DX, Nuyten D, et al. Lung metastasis genes couple breast tumor size and metastatic spread. Proc Natl Acad Sci U S A. 2007; 104(16):6740–5. Epub 2007/04/11. [PubMed: 17420468]

36. Allington TM, Galliher-Beckley AJ, Schiemann WP. Activated Abl kinase inhibits oncogenic transforming growth factor-beta signaling and tumorigenesis in mammary tumors. FASEB J. 2009; 23(12):4231–43. Epub 2009/08/20. [PubMed: 19690215]

37. Wo JY, Chen K, Neville BA, Lin NU, Punglia RS. Effect of very small tumor size on cancer-specific mortality in node-positive breast cancer. J Clin Oncol. 2011; 29(19):2619–27. Epub 2011/05/25. [PubMed: 21606424]

38. Sawyers CL, McLaughlin J, Goga A, Havlik M, Witte O. The nuclear tyrosine kinase c-Abl negatively regulates cell growth. Cell. 1994; 77(1):121–31. Epub 1994/04/08. [PubMed: 7512450]

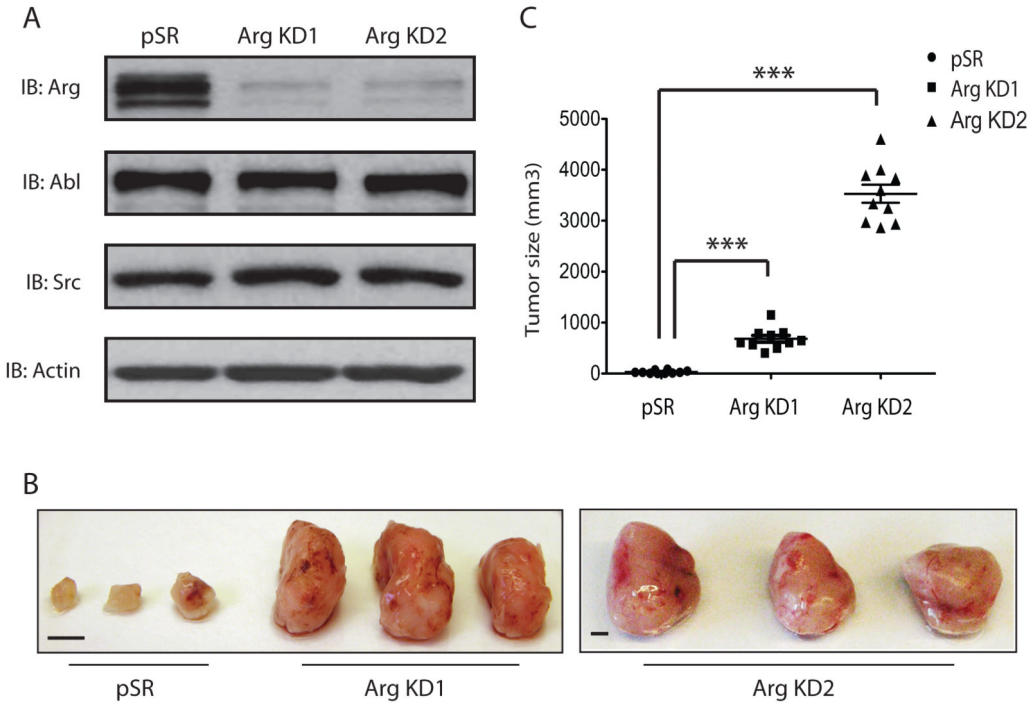

Figure 1. Knockdown of Arg significantly increases MDA-MB-231 xenograft tumor size

(A) Immunoblot showing knockdown of Arg in MDA-MB-231 cell lines by two different shRNA sequences, Arg KD1 and Arg KD2 relative to control empty vector-expressing (pSR) cells. Note that Arg knockdown does not affect expression of the closely related Abl or Src kinases. Actin is used as a loading control.

(B) Orthotopic xenograft tumors were generated with MDA-MB-231 breast tumor cells, stably expressing either control empty vector (pSR) or shRNA for the Arg gene (Arg KD1 and Arg KD2). Mice were dissected and tumors isolated at 8 weeks following injection into mammary glands. Representative tumors from control and Arg KD1 mice are shown. Scale bar: 4mm. (C) Tumor size was calculated at 8 weeks post-injection of pSR control of Arg KD1 cells. n=10 mice per group, ***p<0.001 (Student's t-test), Error bars: Mean ± SEM.

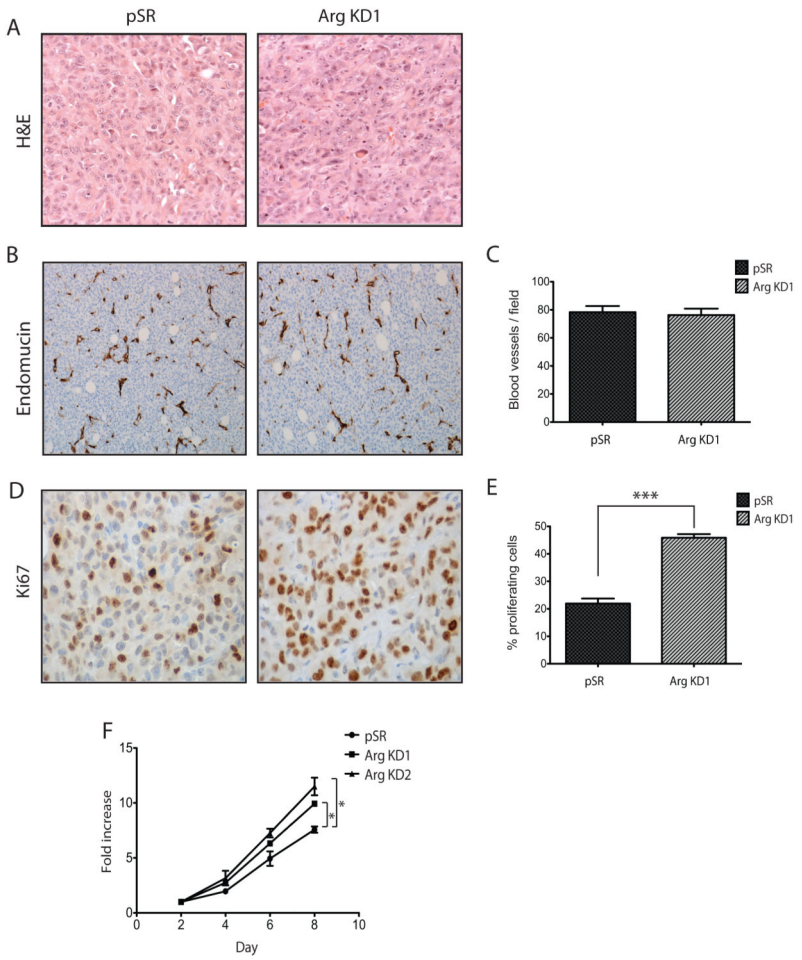

Figure 2. Enlarged size of Arg knockdown tumors results from increased proliferation

Orthotopic primary tumors generated from MDA-MB-231 pSR control or Arg KD1 cells were grown to same tumor size (1-1.2cm diameter).

(A) Representative images of H&E histological staining from control (pSR) and Arg KD1 tumors (magnification 20x).

(B) Representative images and (C) quantification of blood vessels by endomucin immunohistochemical staining from the above tumors (magnification 10x). Shown is the number of blood vessels per field, N=3 tumors per condition, 5 random fields.

(D) Representative images and (E) quantification of proliferating cells by Ki67 immunohistochemical staining (magnification 40x). The average % of proliferating cells in total cells per field is shown. n=3 tumors per condition, 5 random fields per tumor imaged at 40x, ***p<0.001 (Student's t-test), Error bars: Mean ± SEM.

(F) Quantification of pSR control, ArgKD1 and ArgKD2 cells growing *in vitro*. Shown is the average fold increase of cell number in the indicated days over the number of cells over time. n=3 different experiments in duplicates per cell line, *p<0.05 (for control vs. both Arg KD1 and Arg KD2 at Day 8), Error bars: Mean ± SEM.

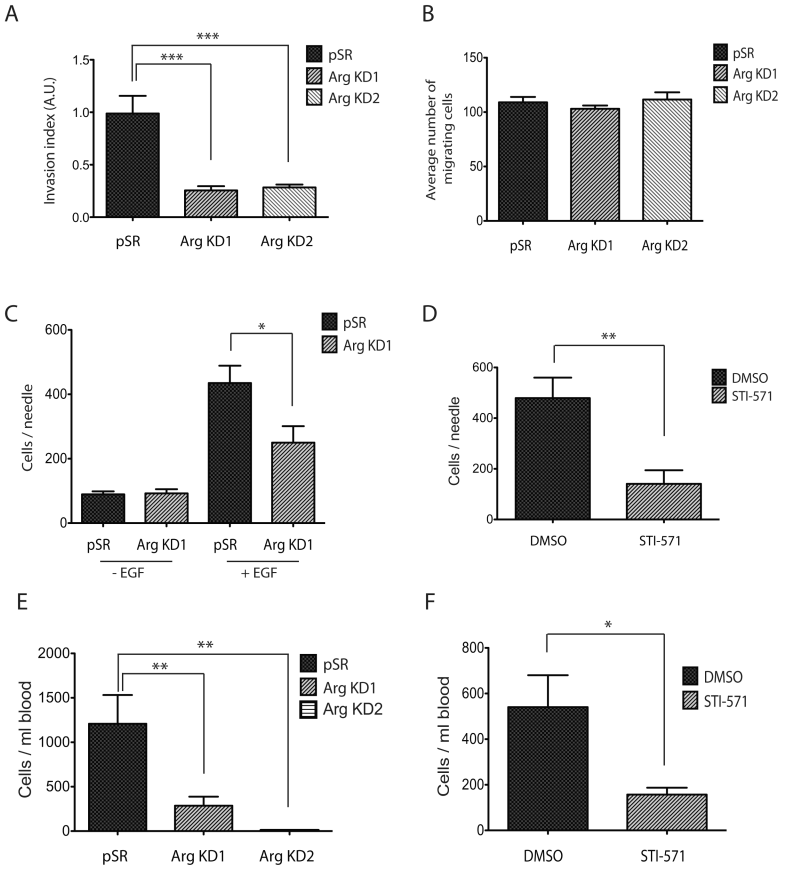

Figure 3. Knockdown of Arg decreases invasion and intravasation of breast tumor cells

(A) Control or Arg knockdown cells were plated on Matrigel-coated membranes and allowed to to invade for 24 hours. Invasion index is calculated as number of cells that migrated through Matrigel-coated membranes divided by number of cells that migrated through uncoated membranes. n=16 for pSR controls, n=14 for ArgKD, ***p<0.001 (one-way ANOVA), Mean ± SEM.

(B) Same experiment as in panel (A), but with uncoated membranes as control for migration. n=16 per group.

(C) *In vivo* invasion towards EGF was measured in orthtopic primary tumors generated with either the pSR control or the Arg KD1 cells. Total cells were counted by DAPI staining. n=4 mice for pSR, n=14 mice for ArgKD1, *p<0.05 (Student's t-test), Mean ± SEM.

(D) *In vivo* invasion towards EGF was measured in orthotopic primary tumors generated with parental MDA-MB-231 cells. Mice were injected with either DMSO vehicle control or STI-571 4 hours prior to the experiment. n=3 mice, *p<0.01 (Student's t-test), Mean ± SEM.

(E) Intravasation was measured as total circulating tumor cells in the blood of mice bearing equal diameter orthotopic tumors of either control, Arg KD1, or Arg KD2 cells. n=9 mice for pSR, n=13 mice for Arg KD1, n=10 mice for Arg KD2. **p<0.01 (Student's t-test), Mean ± SEM. (F) Intravasation was measured in orthotopic primary tumors generated with parental MDA-MB-231 cells. Mice were injected with either DMSO vehicle control or

STI-571 4 hours prior to the experiment. n=11 mice for DMSO control, n=7 mice for STI-571, *p <0.05 (Student's t-test), Mean ± SEM.

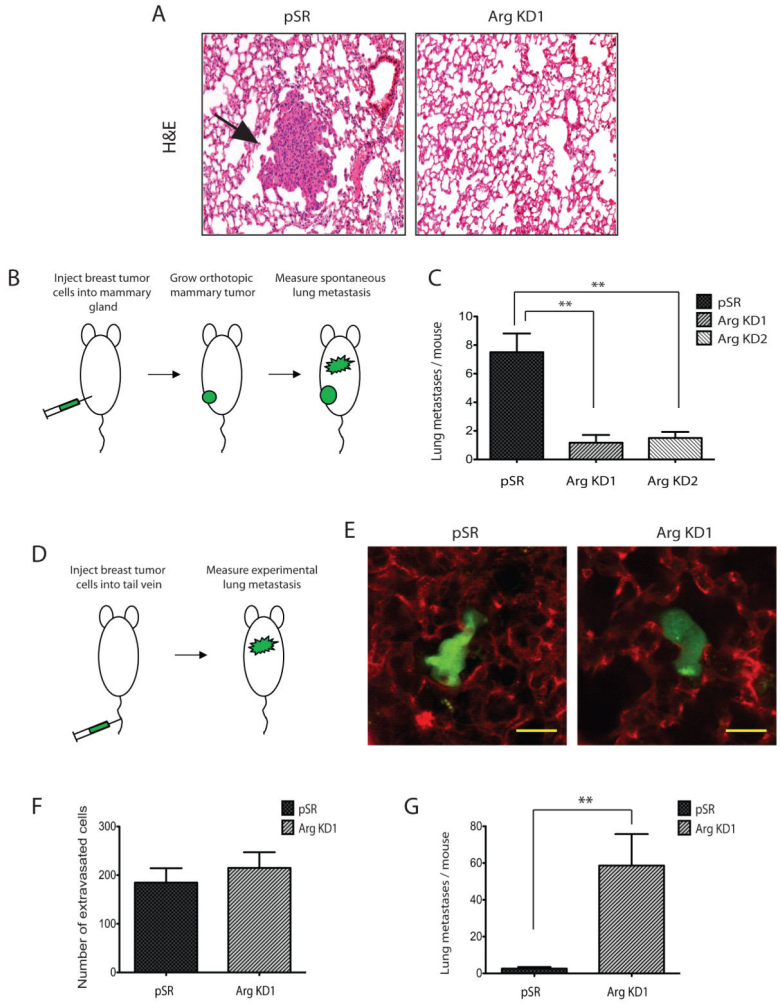

Figure 4. Arg knockdown decreases spontaneous lung metastasis while increasing experimental metastasis

(A) Representative images of lung sections from control and Arg knockdown tumor-bearing mice labeled with H&E.

(B) Cartoon and (C) Quantification of spontaneous lung metastasis by histological examination of metastatic colonies from orthotopic tumors generated either with pSR control or Arg KD1 MDA-MB-231 cells. n=6 mice per condition, *p<0.05 (Student's t-test), Mean ± SEM.

(D) Cartoon and (E) Representative images of single extravasated tumor cells in the lung at 48 hours following tail-vein injection of equal numbers of pSR and Arg KD1 MDA-MB-231 cells to mice. Tumor cells were labeled with tracker dye (green), while lung blood vessels were labeled by rhodamine-conjugated lectin (red). Magnification: 50x. Scale Bar: 20μm.

(F) Quantification of experimental lung metastasis by multiphoton imaging of single extravascular tumor cells at 48 hours following tail-vein injection of equal numbers of pSR and Arg KD1 MDA-MB-231 cells to mice. Shown is average number of single extravasated tumor cells in the largest lung lobe of each mouse, n=5 mice per condition, **p<0.01 (Student's t-test), Mean ± SEM.

(G) Quantification of experimental lung metastasis by histological examination of metastatic colonies at 4 weeks following tail-vein injection of equal numbers of pSR and Arg KD1 MDA-MB-231 cells to mice. n=5 mice per condition, **p<0.01 (Student's t-test), Mean ± SEM.

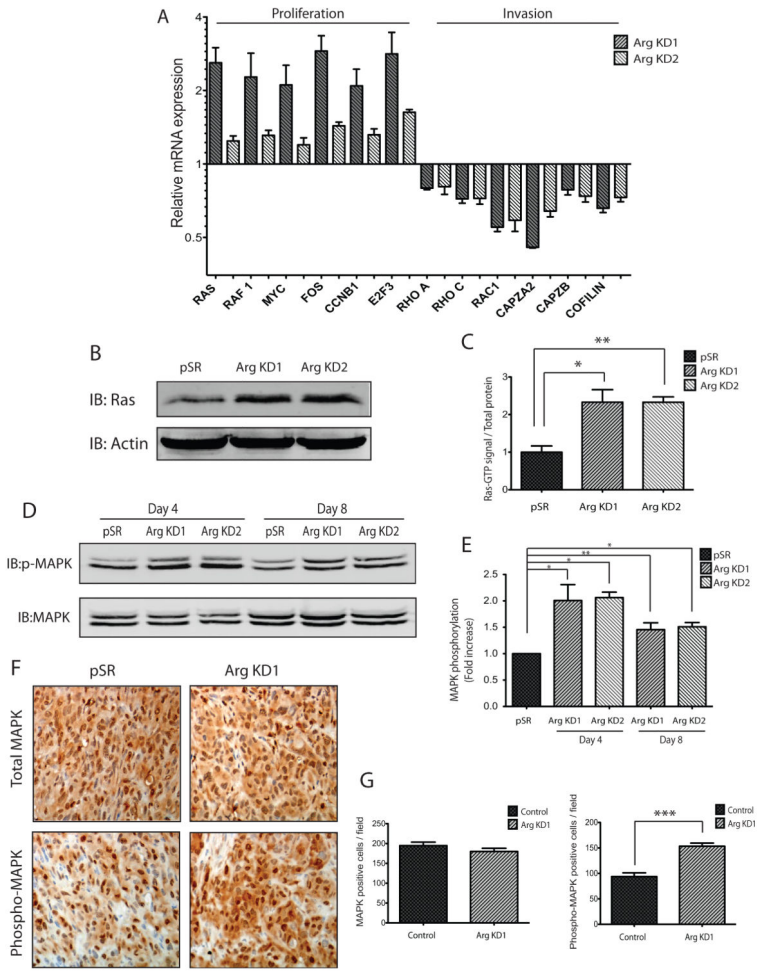

Figure 5. Expression of genes in the invasion and proliferation pathways is differentially regulated in the absence of Arg

(A) mRNA expression was analyzed by real-time PCR in the pSR and the knockdown Arg KD1 and Arg KD2 MDA-MB-231 cells. Results are plotted as fold expression of the knockdown lines relative to the pSR control line. All results shown here are statistically significant. n= 3 replicates for each sample/gene combination, *p<0.05 (Student's t-test), Mean ± SEM. Measurements of all genes tested are shown in Table S1.

(B) Representative immunoblot of total Ras in control pSR and Arg knockdown cell lines (Arg KD1 and Arg KD2). Actin was used as a loading control.

(C) Quantification of Ras activity in the Arg KD1 and Arg KD2 cells lines compared to the pSR control. n=3 per condition, *p<0.05, **p<0.01 (Student's t-test), Mean ± SEM.

(D) Representative immunoblot of phosphorylated and total MAPK in pSR control, Arg KD1 and Arg KD2 cell lines at day 4 and day 8 following plating.

(E) Quantification of fold increase in MAPK phosphorylation relative to control cells. Data are from three independent experiments. n=3 per condition, *p<0.05, **p<0.01 (Student's t-test), Mean ± SEM.

(F) Representative images from immunohistochemistry of pSR and Arg KD1 cell derived orthotopic tumors for total and phosphorylated MAPK. Positive staining for the antibody is

shown in brown, total nuclei were lightly counterstained with hematoxylin shown in blue. Magnification: 40x.

(G) Quantification of total MAPK and phospho-MAPK staining in pSR control and Arg KD1 orthotopic tumors (as shown in panel F). n=6 fields per tumor, 3 tumors per condition, *p<0.05, **p<0.01 (Student's t-test), Mean ± SEM.